Smart Health 32 (2024) 100468

Contents lists available at ScienceDirect

Smart Health

journal homepage: www.elsevier.com/locate/smhl

TinyMSI: A cost-effective handheld device for non-contact diabetic wound monitoring

Alexander Gherardi *, Tianyu Chen, Huining Li, Jun Xia, Wenyao Xu

Department of Computer Science and Engineering, University at Buffalo, United States

ARTICLE INFO

Keywords:
Multispectral imaging
Mobile health

ABSTRACT

Devices characterizing diabetic foot ulcers and other wounds currently fall into two categories. Expensive clinically-oriented devices that use mature technologies such as X-ray CT and hyperspectral imaging or low-cost solutions that leverage deep learning to infer wound characterization from conventional smartphone camera images or simple surrogate markers. Mature medical-grade devices are too expensive for primary care and assisted living facilities. Low-cost solutions rely too much on indirect statistical inference to be clinically suitable. Therefore, we propose a device that leverages mature, clinically suitable optical technologies to provide a solution for these facilities. Recognizing that individual combinations of 1–2 bands of active illumination are used individually to capture pulsation, vascular, and oxygenation images. We combine all these bands into a single multispectral lighting source to create a multi-functional, reliable device for wound assessment. We selected these bands to leverage CMOS cameras near orthogonality between the RGB channels and leverage that CMOS cameras can also sense near IR light if a filter is not present, reducing overall system complexity and needed bands. For each function, the necessary lights are turned on, and the captured raw video is then fed to the corresponding sequence of image processing steps. No deep learning models are used, so large training datasets are not required. Our device is also small, lightweight, and handheld.

1. Introduction

Diabetic foot ulcers (DFU), which are exposed wounds that develop on the foot, may seem harmless but are stunningly lethal. 5-year mortality rates exceed 25% in individuals who experience complications (Armstrong et al., 2020), according to one study. Contributing to these bleak outcomes, foot ulcers are commonly related to nephropathy disorders, which impact the mobility of these people with diabetes (Delbridge et al., 1988), making them less inclined to seek out regular treatment and monitoring. Outcomes for individuals with diabetic foot ulcers, like many other medical conditions, are often better when interventions are prompt. For those with limited mobility, getting to a clinic can be impractical, and home visits from clinicians can be expensive, leading to delayed discovery of infections and complications in the healing process (Pérez-Panero et al., 2019) and causing a greater burden to medical professionals.

In clinical settings, CT anagrams and X-rays (Bearden, 1967) are used to monitor DFU, but this equipment is large and requires several highly trained individuals to use, maintain, and interpret the results of scanning. This makes it expensive and only possible to use in large hospitals or highly specialized clinics. Hyperspectral imaging and Near Inferred spectroscopy (Ng & Simmons, 1999) are positioned as a lower-cost and more compact alternative to CT. Although optical technologies (Erickson & Godavarty, 2009) are

* Corresponding author.
E-mail address: ajgherar@buffalo.edu (A. Gherardi).

https://doi.org/10.1016/j.smhl.2024.100468
Received 15 March 2024; Accepted 18 March 2024
Available online 26 March 2024

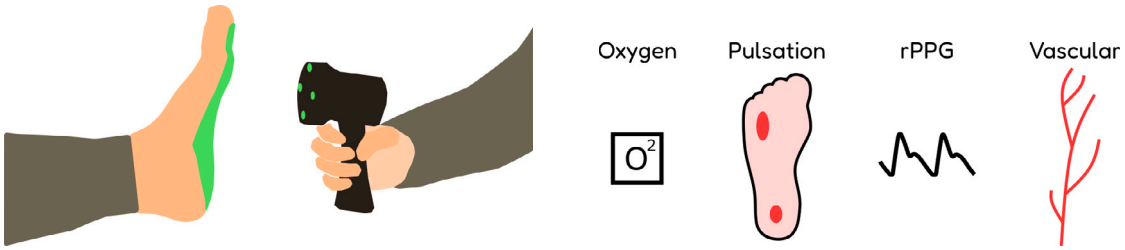

Fig. 1. TinyMSI our novel handheld system for wound assessment (a) uses polarization and narrowband illumination to see through the skin and produce the necessary images and signals (b) for informed diabetic ulcer care in primary care and community health environments.

non-contact and relatively easy to use, they are prohibitively expensive for primary care settings and community health centers due to the large array of narrowband lighting sources required or specialized cameras.

For home care, there has been an effort to create low-cost optical technologies that can be used to monitor and track biological signals relevant to DFU and general wound healing (Moraitou et al., 2017). Many algorithmic solutions can produce decent-quality PPG signals with just a webcam and ambient lighting. And SpO2 monitoring can be done with only a smartphone and its flash (Li, Zheng, Pandya, Xu, Xia, Xu, 2022). These low-cost optical solutions are capable but entirely outclassed by HSI (Lu et al., 2020) and NIRS regarding spatial resolution and clinical suitability. All optical solutions, regardless of cost, are also fractured, with each system only functioning as a specialized tool for monitoring one aspect of the wound, with a clinic needing to purchase and learn several different tools to get the complete picture of the wound's condition.

We propose TinyMSI, a handheld solution that gathers all the information needed to make informed decisions on the condition of a wound. It is a multi-function tool that can capture high spatial resolution vascular, pulsation, and oxygenation images and the rPPG signal (see Fig. 1). It works by using multispectral imaging, where a few narrowband sources of important highly informative wavelengths illuminate the target, providing images with spectral significance at a far lower cost than HSI. TinyMSI is designed to be small, easy to hold, and immediately usable without specialized training required to operate, enabling any primary care professional to gain the insight to assess wounds and ulcers quickly. Furthermore, the multispectral imaging modality is flexible with new combinations of wavelengths, and optical monitoring of other conditions or biomarkers, such as glucose, is possible.

Our major contributions are as follows:

- A novel multispectral hardware and software solution engineered specifically to monitor patient wound vitals.
- A Single Camera Imaging solution that utilizes COTS hardware, keeping costs and area to a minimum.

2. Design rational and insight

In this section, we explore the insight behind our device's overall design. First, presenting the rationale behind the images that our devices capture. Then, outlining the primary considerations that must be addressed when creating a multispectral lighting and imaging system for bio-imaging. Then, we will explore how we solve secondary challenges related to our system and other optical imaging systems.

2.1. Rational

Diabetic foot ulcers are caused and exacerbated by a compendium of underlying issues that are not visible from normal camera images, like flat feet, and symptoms of neuropathy like callus buildup and drying of the skin may be (Oliver & Mutluoglu, 2023). Some of these underlying issues may be coupled, like poor perfusion or peripheral vascular images leading to poor wound oxygenation (Tresierra-Ayala & Rojas, 2017). They need not necessarily be coupled, however. Determining the underlying cause or set of underlying causes is critical for creating and updating an effective treatment plan. This motivates our multi-functional solution, which enables the independent analysis of vascular structure, perfusion strength, and oxygenation in a patient's tissue—allowing practitioners to avoid needing to infer the ultimate cause of a change in a patient's condition or refer the patient to a specialist with more equipment and reducing the financial burden on underprivileged patients and the time needed to get a diagnosis.

2.2. Design considerations

A principal aspect of our design is that it is based on mature optical technologies used to provide each of its capabilities; rather than reinventing each of these methods, it leverages and improves upon them before combining them into a unified system. With that being said, lighting quality is the primary factor in ensuring a good response from the tissue within the skin as most of the images generated by TinyMSI, regardless of the chosen band, leverage the rPPG signal present when a pixel or group of pixels is observed for some time. The quality of the rPPG signal acts as a proxy for the overall quality of the image. Here, we outline the considerations that motivated our lighting source design.

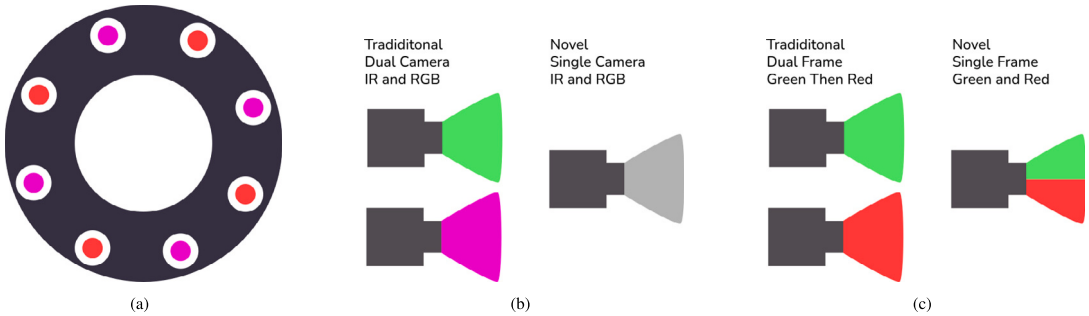

Fig. 2. The novel aspects of TinyMSI. Our system makes use of a circular multispectral lighting design (a) to evenly illuminate the target with various combinations of bands, uses single camera imaging (b) to eliminate the need for a separate IR camera to capture vascular images, and has a novel single frame oxygenation imaging (c) technique to capture the video needed for precise oxygenation imaging at a high frame rate.

2.2.1. Lighting type

Hyperspectral systems utilize special optics and optical bandpass filters to split a CMOS camera into several single-band cameras or capture each needed band, in turn, using a different light source for each. In either case, these systems are costly for 10–20 bands, and for in-turn measurement, the frame rate is too low for PPG. This motivates our use of a multispectral system with only a few critical bands. We avoid complex optics in our design, leveraging having more camera channels than bands to prevent needing to perform in-turn measurements without compromising frame rate.

2.2.2. Lighting bands

We select bands to provide the most information with the most minor post-processing and power wasted. Green is a commonly used band for PPG and pulsation sensing as the blood has a high absorption coefficient for green light, requiring less light for increased sensitivity. For oxygen sensing, we utilize red and green light to provide the two bands necessary for determining the concentration of two materials in a sample optically; these bands were chosen to be orthogonal with respect to the camera and significantly different from each other in the spectral response of oxygenated hemoglobin. We utilize near IR light for vascular sensing as its sensitivity to hemoglobin is high and has a high penetration depth.

2.2.3. Lighting polarization

Using orthogonal polarizers to reduce specular reflections from the skin surface and maximize reflected energy from the skin tissue is commonplace in the literature. We incorporate this into our design with a film over the lights and the camera. Using polarizers drastically reduces the reflected energy from the subject, making it difficult to fully utilize the dynamic range of the camera without very long exposure times or more analog gain.

2.3. Design challenges

2.3.1. Frame rate

Reliable PPG sensing requires a frame rate higher than the Nyquist rate of the PPG waveform and high enough to enable spectral filtering. However, in traditional multispectral/hyperspectral systems, each band is captured in turn, reducing the frame rate drastically. Furthermore, the camera's exposure time can only be made so high before the frame rate is decreased. To address this, we record all necessary bands simultaneously rather than in turn and use a high-aperture lens to reduce the needed exposure time.

2.3.2. Information coupling

The spectral response of RGB CMOS cameras is not perfectly orthogonal across the three channels. This means that, for example, illumination from a lighting source with a green wavelength would create a significant response in the Green Channel but also a minor response in the Red and Blue channels. This spectral mixing property, however, can be perfectly compensated for when the number of simultaneous lighting bands used is equal to or fewer than the channels lighting using the spectral mixing coefficients from the camera's datasheet.

3. Imaging design and principle

In this section, we explore novel aspects of our imaging system that reduce the system's complexity and enable higher performance, namely our single-camera imaging system and single-frame oxygen image (see Fig. 2).

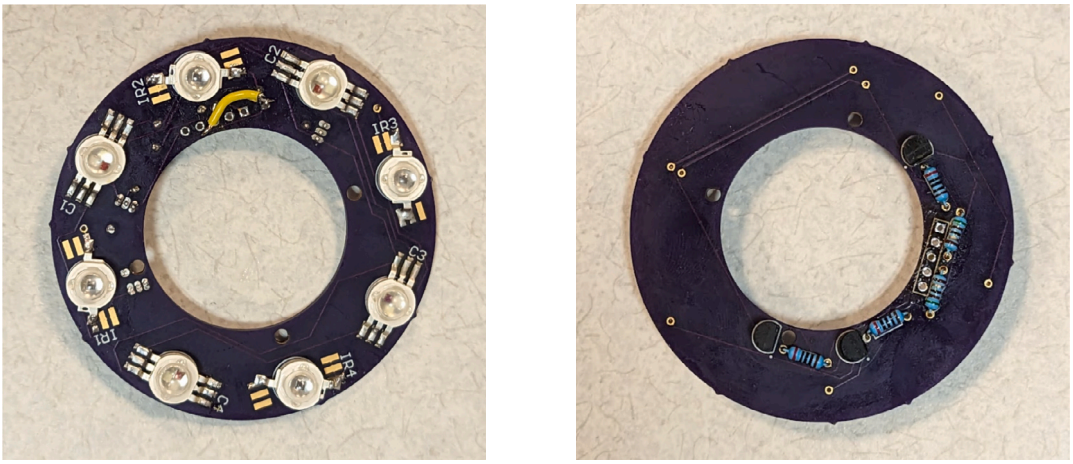

(a) (b)

Fig. 3. Views of the Lighting PCB showing all lighting components. The front of the PCB (a) contains the circular alternating arrangement of NIR and RGB LEDs. The back of the PCB (b) contained the MOSFET transistors used for switching and other passive components used for current regulation.

3.1. Single camera imaging

A key aspect of the system's hardware is its single-camera imaging setup. Optical systems used in labs tend to utilize two cameras for imagining involving IR and color sources. This is because, normally, color cameras have IR blocking high pass filterers; color cameras possess this to prevent noise from ambient IR (the largest of which is the sun) sources from perturbing the image, as every color channel is mildly sensitive to IR in normal commercial cameras. IR cameras are used alongside filtered color cameras to capture IR images, but this causes the additional expense of an IR camera to be necessary. So, we propose a different application-specific solution since vascular images require IR but other TinyMSI images do not. The operation of the device can be separated into two modes. A vascular capture mode with only the IR LEDs powered on to detect veins, and a general mode in which the combinations of visible bands are powered on to detect tissue oxygenation and blood pulsation using a single non-IR filtered color camera. This separation is aided by the reasonable assumptions accompanying the use of the device, that being that the user is not outside as nearly half the sun's light is in the IR band and that the lights are dimmed inside, as some indoor lights also generate IR as a byproduct. Any stray IR can appear as color-distorting noise in general mode, but environmental IR is minimal when the use assumptions are met.

3.2. Single frame oxygen image

Oxygen imaging using hyperspectral imaging is now commonplace in the literature (Saiko, Lombardi, Au, Queen, Armstrong, Harding, 2020). But as mentioned earlier, hyperspectral imaging requires expensive bandpass filters or slow in-turn imaging by cycling bands. To alleviate these concerns, our device uses a new technique in which red and green lights are on simultaneously during every oxygenation frame. As these wavelengths are nearly orthogonal in the color space of our Off-the-Shelf camera (and the true red and green can be recovered with a linear system using the pixels sensitivity to each wavelength and observed response), the device imaging system can, in this mode be regarded as two distinct ones, a red sensing camera and light, and a green sensing camera and light. These two "virtual" cameras simultaneously capture the frames needed for a dual-wavelength oxygen image.

4. Device

Here, we discuss the TinyMSI hardware itself and its parameters, which leverage the ideas developed in the previous sections. We examine the physical design of the system as well as the specifics of the camera and lighting system with a specific focus on noise.

4.1. Camera design

Our camera the FLIR Blackfly S USB3 BFS-U3-13Y3C-C and lens the Fujinon 1.5MP 6 mm C Mount were selected to ensure high SNR as the capabilities TinyMSI offers benefit from lower noise. The camera noise can be broken down into a few key categories.

Fig. 4. The side profile of the TinyMSI with labeled height and width dimensions. Highlighting the ergonomic design of the 3D printed enclosure and the resemblance of the device to other common handheld devices like Camera Gimbals and Thermal Cameras.

Table 1
Camera parameters.

Parameter name	General mode value	Vascular mode value
Aperture	f1.2	f1.2
Exposure Time	12 – 25 ms	35 ms
Frame Rate	24 Hz	N/A
Analog Gain	0–5 dB	0 dB
Focal Length	6 mm	6 mm
Gamma Correction	Off	Off
Color Correction Matrix	Off	Off
AWB and AE	Off	Off

4.1.1. Random photon noise

also known as shot noise, is caused by the random nature of photons; as the number of photons being integrated by a pixel follows a Poisson distribution, there is statistical noise just from the nature of light itself. Larger pixels reduce shot noise as they integrate more photons. Longer exposure times also reduce shot noise.

4.1.2. Circuit noise

Cameras have internal circuitry to amplify the signals received from each pixel so that they can be digitized using the full range of the camera ADC. The noise from amplifiers in the camera worsens as the amplifiers are set to higher gains. So, higher exposure times are preferable to increases in analog gain.

4.1.3. Quantization noise

As the PPG signal is very minute relative to the DC signal and specular reflections from the subject's skin, quantization noise becomes the primary source of noise in the system. To overcome this noise, it is best to fully use the camera's dynamic range by increasing the integrated light through various means and having a higher bit depth ADC.

Automatic white balance and Auto exposure do not generally choose the optimal setting for use with rPPG. So those are disabled, and gamma correction causes non-linearity in the signal as well. Built-in Color Correction Matrices assume broadband light sources and are also unsuitable here. Table 1 summarizes the parameters we determined.

4.2. Lighting design

As explored earlier, our system is built around a polarized multispectral array with three bands: Near IR, Green, and Red. In creating our design, we aimed to optimize the uniformity and ensure high enough intensity to utilize the full dynamic range of our camera. To do this, our design uses a circular arrangement of LEDs alternating between Near IR and a combination of Red and Green LEDs. These LEDs are high power capable of using injection currents of up to 300 mA each. At a distance of about 0.5 m from the camera, the wash from the LEDs is roughly uniform and covers the entire target area. The LED array is approximately co-planer with the front of the camera lens. The LED array is switched from a high-current 5v regulated source derived from USB power to the lighting system by MOSFET transistors controlled by 5v low-current lines.

4.3. Physical design

The system is housed in a 3D-printed enclosure with design elements drawn from handheld thermal cameras and speed measurement devices (see Fig. 4). A cylindrical barrel contains the FLIR camera module, a simple high aperture machine vision lens, a custom PCB implementing the lighting system (see Fig. 3), and an Arduino Nano Every for controlling the lighting system. Two USB connectors come from the back of the device to connect the Arduino and FLIR to a computer for data processing and system configuration. An ergonomic handle is present underneath the main barrel to make holding comfortable. Two circular cutouts comprise an orthogonal polarization filter on the front of the cylindrical barrel.

5. Image processing

After illuminated images are streamed from the camera they are processed into one of four products used to evaluate patient blood perfusion (pulsation, oxygen, vascular, rPPG). Before processing, the images are segmented using k-means on the green channel using a large k-value to increase segmentation granularity and remove background pixels, ensuring that the tissue does not blend into the background.

5.1. Remote PPG

To get the PPG in a non-contact way, we utilize red and green light. Images are first segmented, then all pixel intensity values corresponding to a channel within the region of interest are averaged, and the blue channel is discarded, yielding two time-series signals by tracking this ROI mean. These signals are then filtered using a bandpass filter to remove noise and the effects of the respiration signal. Lastly, independent component analysis is used with the fully filtered red and green signals to refine the signal further. While some papers use the ICA method with constraints (Macwan et al., 2018) to remove the interference from the skin, our polarization imaging method accomplishes that already.

5.2. Pulsation image

To ascertain the pulsation strength in the foot surface tissue a green image stream is used (Kumar et al., 2020). The images were aligned with each other to compensate for motion using an optical flow algorithm. An averaging filter is convolved with each image to reduce the noise from quantization and random camera noise. At each observed pixel, small fluctuations in the reflected light from the surface of the foot form a time series signal that is correlated with the cardiovascular dynamics in the tissue corresponding to that pixel. To extract these dynamics, the image stream is regarded as a collection of time series signals observed by each pixel in the camera $P(x, y, t)$ from frames between time T_0 and T_1 sliced from the original stream; these signals are then normalized in a way that makes the image invariant to uneven lighting and non-cardiovascular dynamics in the tissue. This is done using two band-pass filters, one from 0.5hz to 5hz to get an "AC" signal and the other from 0 to 0.3 hz to get the "DC" signal. The AC signal is then normalized by the DC signal to obtain the skin response signal R as below:

$$R(x, y, t) = \frac{AC}{DC} = \frac{P_{0.5hz-5hz}(x, y, t)}{P_{0hz-0.3hz}(x, y, t)}, \tag{1}$$

$$F(x, y) = \frac{\langle R(x, y, t),\ PPG(x, y, t)\rangle}{\langle PPG(x, y, t),\ PPG(x, y, t)\rangle}. \tag{2}$$

The pulsation strength at each geometric pixel is then extracted by computing the inner product between the skin response signal R. An out-of-channel PPG signal is captured using a contact optical PPG sensor or by averaging the skin signal R over the entire visible tissue for a non-contact option, these PPG signals are filtered from 0.5 hz to 5 hz then normalized using the Hilbert transform before being used. The inner product result captures the correlation between the PPG signal, which is the pulsation of the entire tissue, and each individual skin response signal R signals with higher magnitude correlated components have higher pulsation magnitudes. The pulsation magnitudes are arranged back into a frame F to visualize pustule dynamics throughout the tissue. The inner product can be computed using a sliding window of source frames to enable a real-time pulsation view.

5.3. Oxygenation image

Calculating the oxygen saturation directly using absorption spectroscopy has some limitations; primarily, getting the necessary calibration images using a white and black reference can be difficult when polarization filters are used. The alternative to polarization imaging would be to model melanin absorption directly, but this requires more wavelengths to be used, which drives up the cost, causes higher SNR, and precludes the oxygenation from being captured with the same device as the pulsation since the pulsation requires polarization filtering. So, rather than directly modeling the oxygen saturation, we instead fit a quadratic model to get the SpO2. This is a common method in the literature for obtaining the SpO2 value from just two different measured amplitudes captured at different wavelengths. We observe that this method can be applied pixel-wise to a pair of images captured at two different wavelengths.

Using our single-camera oxygenation imaging technique, we obtain the necessary red and green frames to compute the oxygenation saturation at each location in the visible tissue. That is the ratio of oxygenated hemoglobin HbO2 to non-oxygenated

Table 2
PPG signal analysis functions.

Function	Description	Formula
Motion Artifact	Calculates the average absolute difference between adjacent PPG samples, highlighting motion-related artifacts.	$A = \frac{1}{N}\sum_{i=0}^{N-1} \lvert x[i+1] - x[i] \rvert$
Pulse Height Variability	Measures variability in pulse peak heights, providing insights into amplitude fluctuations within the signal.	$PHV = \sigma(h)$
Pulse Width	Computes the average time between pulse peaks in a signal, offering temporal characteristics of the pulsatile waveform.	$W = \frac{1}{N}\sum_{i=1}^{N-1} \frac{t[i+1]-t[i]}{f_s}$
Heart Rate (BPM)	Estimates heart rate in beats per minute through peak counting, a fundamental metric for physiological assessment.	$HR = \frac{N_{peaks}}{T}$
Heart Rate Bandwidth	Assesses the frequency bandwidth of the heartbeat using the power spectrum derived from FFT analysis.	$BW = f_{high} - f_{low}$
Kullback Leibler Divergence	Measures the dissimilarity between two power spectral density estimates, indicating information loss or difference in signal characteristics.	$KL = D_{KL}(P_1 \lvert\lvert P_2)$
FFT MSE	Computes the mean squared error between FFT magnitudes of two signals, quantifying their spectral similarity or dissimilarity.	$MSE = \frac{1}{N}\sum_{i=0}^{N-1} (Y_1[i] - Y_2[i])^2$

hemoglobin Hb. Just as in the pulsation image, we first align a group of successive pairs of green and red images using optical flow, perform a spatially averaging convolution to reduce noise, and regard the values associated with a pixel (x, y) as a time-series P_{Red} and P_{Green}. We also AC/DC normalize both of these images using band-pass filters to obtain the normalized reflectivity R for each channel as the blood flow dynamics are still present in both channels and perform lock-in amplification by normalized inner product with ground truth PPG from a contract PPG sensor just as in pulsation imaging. Then, to obtain the SpO2 value, we fit a quadratic model to the ratio of the two normalized images (rim Park et al., 2023). To determine the model's coefficients, a pulse oximeter is used for ground truth, and the model is optimized such that the spatial average of an ROI near the oximeter has the minimum error. The model can also be fit for various exposure settings to enable the Auto Exposure as below.

$$\mathrm{SpO2}(x, y, t) = a\left(\frac{F_{\mathrm{Red}}}{F_{\mathrm{Green}}}\right)^2 + b\left(\frac{F_{\mathrm{Red}}}{F_{\mathrm{Green}}}\right) + c. \tag{3}$$

5.4. Vascular image

Near-infrared (NIR) illumination and imaging techniques can be employed for non-invasive visualization of superficial human vasculature (Shin & Lee, 2018). NIR light between 700–900 nm wavelengths can penetrate sufficiently deep into skin tissue to reach subcutaneous vessels while remaining unaltered by absorption from melanin. However, the contrast and resolution of raw vascular images acquired through NIR photography tend to be poor owing to significant optical scattering events and limitations of digital camera sensors. To address these factors, post-processing of the NIR images can be performed through a vessel enhancement algorithm known as Sato's method (Sato et al., 1998).

Sato's method calculates the eigenvectors v and eigenvalues λ of the Hessian matrix H, which captures all the second derivatives at a given pixel and uses a detector function that is maximized when the eigenvalues indicate that in one direction, the direction of the tube there is minimal change and that in the other direction the direction orthogonal to the tube the change is maximized. That is the function in Eq. (4) shown below captures the likeness of a given neighborhood around a pixel to a tube. Compiling each pixel's likeness values into an image reveals the vasculature for clinical evaluation:

$$T(x, y) = \lambda_2, \tag{4}$$

where λ_n is the nth smallest eigenvalue of H(x, y).

5.5. Graphic user interface

The TinyMSI recording capabilities were made accessible from a custom GUI that gave users a real-time view of the camera output, select the desired camera function, and record timestamped video with embedded patient biographical information.

6. Evaluation

In this section, we evaluate our device's performance in its various capabilities. We begin by evaluating the device's rPPG capability since rPPG is used downstream when generating the pulsation and oxygenation images. Then, we further verified that expected physiological features and behaviors were present in the pulsation and oxygenation images. Lastly, we evaluate the vascular imaging capability by comparing extracted features from the left to right hand.

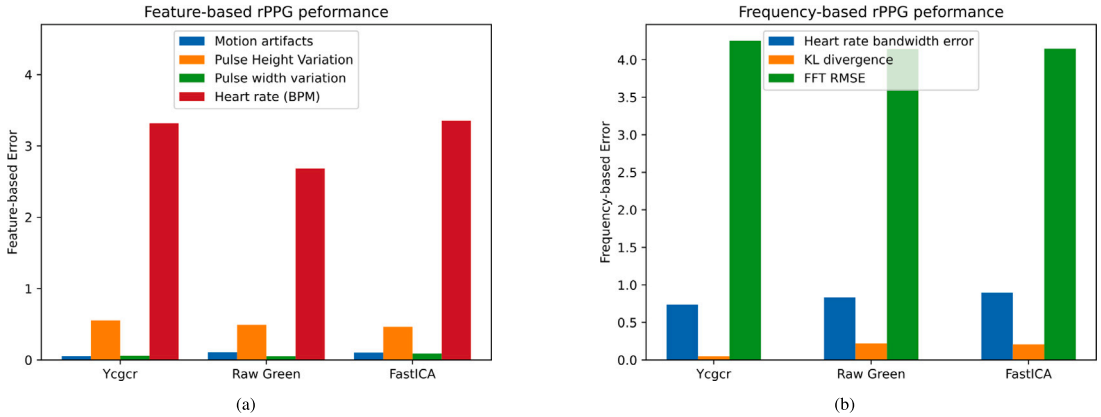

Fig. 5. TinyMSI rPPG performance metrics. Feature-based error (a) across four different features determined by signal comparison with a reference contact PPG signal and frequency-based error (b) across three different frequency features. Three different ways of extracting rPPG from a preprocessed sequence of images are compared.

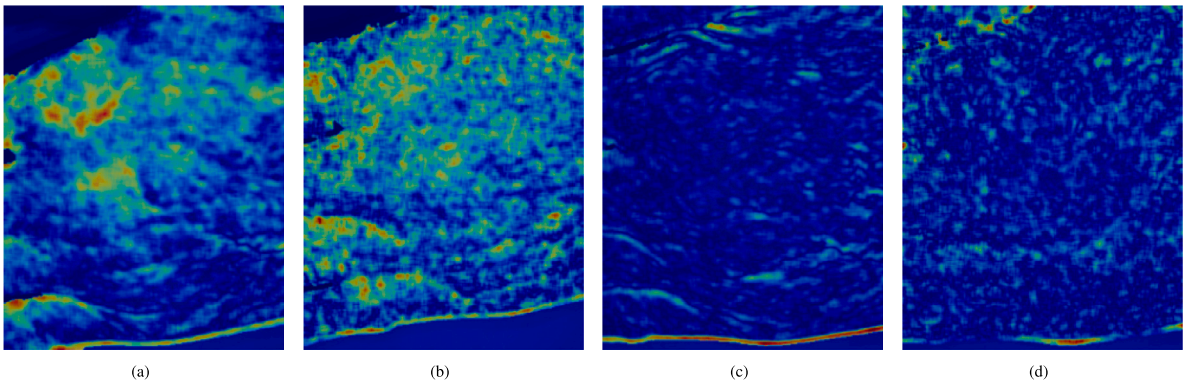

Fig. 6. The TinyMSI pulsation image capability is highly sensitive and can resolve hand circulation changes caused by applying pressure around the forearm in 20 mmHg increments. With 0 mmHG (a), 20 mmHG (b), 40 mmHG (c), and 60 mmHG (d) applied pressures shown.

6.1. rPPG

To evaluate rPPG performance, we use two categories of metrics. Signal metrics and physiologically relevant metrics (see Table 2). The signal is first segmented into several segments, each lasting 10s. Z-standardization is then applied to ensure that signal evaluation is independent of local measurement and scaling. Then, traditional signal metrics are used to quantify the error, considering metrics like KL divergence, Mean Squared Error, and persons' r metric for correlation. Additionally, psychologically relevant metrics are used to quantify the error in things like beats per minute (BPM) and pulse width/height. Together, the metrics allow judgments to be made about the intensity of signal artifacts, baseline drift, and other signal defects and ensure the signal is related to the dynamics in the subject's limb.

To collect the rPPG data, subjects were instructed to place their hands face down on a table's surface and keep still, keep their other hand still in their lap, sit upright in the chair, and breathe normally. The TinyMSI device was also attached to a 3D-printed arm to keep it still. The collection lasted one minute per subject. Ground truth data was collected with the Analog Devices MAXREFDES103 watch evaluation device worn on the subject's opposite hand during collection. The watch has red, green, and near IR bands like the TinyMSI device. Data from TinyMSI and the watch were synchronized using the provided Unix timestamps. Two subjects were collected, and the resulting metrics were averaged.

From Fig. 5, it can be seen that the suite of extracted metrics TinyMSI exhibits small to medium error depending on the selected metric. With heart rate error being the easiest to compare, we can see that the 3 BPM error of our system is in line with other comparable systems for extracting rPPG (Haugg et al., 2022).

6.2. Pulsation image

To evaluate the quality of the pulsation image capability, we use an experimental protocol similar to the one we used in the rPPG evaluation. Again, the subject was instructed to keep still and wear the reference watch on their opposite hand. Here, however, a

Fig. 7. The intermediate ratio of ratios image used to calculate the oxygenation image. Variations can be seen around the edges of the fingers which is consistent with the expected psychological behaviors.

blood pressure cuff was placed around the arm of the subject corresponding to the hand being observed using TinyMSI. Four images were recorded in a progression of pressure levels starting at 0 mmHg and increasing by 20 mmHg with each successive image. For each image, 1 min of synchronized video was recorded to perform the calculation.

The output images were 2D plotted using the same color scale next to each other so they can be evaluated together; the result can be seen in Fig. 6. It can immediately be seen that when the pressure is increased, there is weaker blood pulsation across all visible tissue. Consistent with pulsation images captured using Kamshilin et al. (2011) it can be seen that there are large pulsation hot spots that disappear as pressure is increased. Which is the expected behavior.

6.3. Oxygenation image

To evaluate the relevance of our oxygenation image, we evaluate the qualitative similarities between our oxygenation image captured in a normal subject under normal conditions and the expected oxygenation patterns determined by understanding the physiological pattern between tissue oxygenation and local vascular structure.

The tips of the fingers and the upper half of the palm are known to have a higher level of oxygenation compared to other parts of the hand, as the fingers are surrounded by the proper digital artery and the proper common digital artery, which transport a large amount of oxygen throughout the area (Ruengsakulrach et al., 2001). High blood flow through proper palmar digital arteries also provides a significant oxygen supply to the fingertips and upper palm. Previous works have shown through near-infrared (NIR) oxygen imaging that the fingers and edge around the palm carry higher oxygen levels than other areas of the hand (Dietrich et al., 2021). This is consistent with known cardiovascular anatomy. The palmar arches provide blood to the proper digital arteries that run along the fingers, providing high oxygenation (Lind & Williams, 1979).

We collected an oxygenation image from a single subject using a protocol similar to the earlier rPPG collection protocol to validate our system. The subject was instructed to keep still and place their palms face down on the table. One minute of simultaneous red/green video was captured along with a ground truth PPG signal from the watch. The video was processed in accordance with the oxygenation imaging pipeline outlined previously. Forgoing the modeling step as it is not necessary for the evaluation of the spatial characteristics of the image.

Evaluating the spatial patterns of oxygenation, we can see strong agreement with established physiological principles of hand vasculature and oxygen supply. This physiological accuracy of the spatial oxygenation patterns validates our imaging system's oxygen measurement capabilities (see Fig. 7).

6.4. Vascular image

We adopted techniques similar to those used in fingerprint analysis to evaluate vascular images from our device. We recorded images from four distinct limbs of two subjects under near-infrared (NIR) illumination. In accordance with Section 5.4 we first applied the K-means algorithm to the NIR frames. Then, we used SATO multiscale filtering to extract the curvilinear structures corresponding to the veins.

In fingerprint analysis, minutiae are key points used to identify the matching between fingerprint images, corresponding to discontinuities in the ridge pattern. To find these minutiae key points in the processed vascular maps, we extracted SIFT (Lowe, 2004) and ORB (Rublee et al., 2011) feature descriptors, which have been used effectively for fingerprint minutiae matching (Zhou

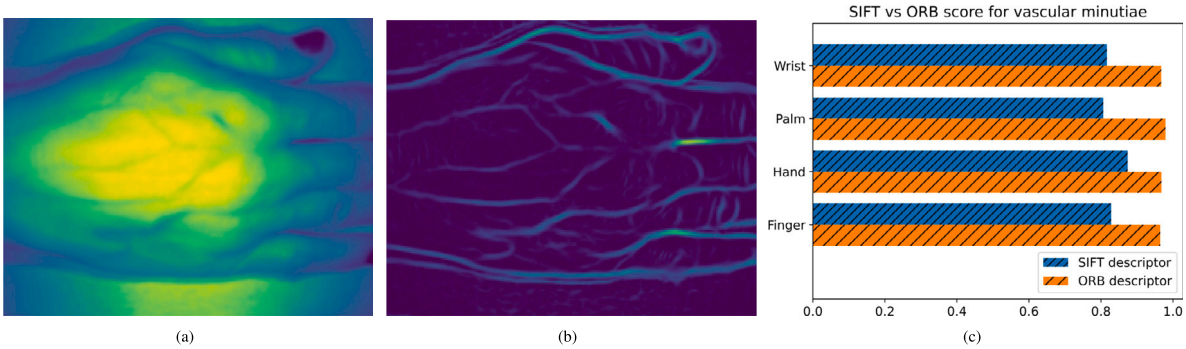

Fig. 8. Raw NIR image (a) captured using TinyMSI and processed vascular image (b) with vessels extracted using a SATO filter. Performance metrics (c) were obtained by comparing vascular minutiae features extracted using SIFT and ORB between symmetric body parts.

et al., 2013). The SIFT descriptor characterizes local gradient information around key points, while the ORB descriptor uses binary features from key points.

After extracting the SIFT and ORB descriptors from the vascular images, we performed L2-norm matching between the 10 vascular maps based on these minutiae descriptors. The L2-norm calculates the Euclidean distance between descriptors, allowing us to match similar minutiae points across the different vascular images. This fingerprint-inspired approach provides an effective way to evaluate and compare the vascular structures captured by our system.

Intuitively, there should be a major similarity between vascular patterns and features in symmetric areas on the body (e.g., right and left hands). Minutia analysis allows us to quantify the degree of similarity in the symmetric pair of processed images captured using TinyMSI. The results are shown in Fig. 8, with nearly all symmetric pairs of images showing higher than 80% similarity scores it is suggestive that the vascular imaging capability of TinyMSI is extracting vascular-related ridges rather than random noise.

7. Discussion and future work

7.1. Other wound information

While the images we capture with the TinyMSI system are highly informative for the treatment of DFU and other wounds, there are other valuable images for the treatment of wounds, such as inflammation, that can be inferred using the images provided by the various modes of TinyMSI. Future work can also investigate using TinyMSI technology to infer moister content by adding a short-wave IR band to the system. As well as augmenting TinyMSI to measure other spectral significant images like glucose maps, for instance.

7.2. Racial bias

Individuals have various melanin concentrations in their skin; our oxygenation imaging system does not account for that, as it only uses two bands. To improve our system robustness in this area, future works can investigate using the observed skin tone without any active illumination as a parameter in modeling or adding more bands to estimate the melanin directly from its spectral response. Contact SpO2 methods have used similar techniques to compensate for skin tone previously.

8. Conclusion

In this paper, we have presented TinyMSI, a handheld device capable of imaging blood vessels, pulse rate, and tissue oxygenation in human skin using multispectral optical sensing.

Our prototype is demonstrated in its capability to extract physiological indicators using different optical techniques. While used for wound monitoring here, these capabilities could be extended to diverse related health applications. For example, detecting irregular heartbeat or hypertension with remote photoplethysmography and generating oxygenation maps to monitor surgical patients. TinyMSI's high resolution could enable early diagnosis by identifying subtle anomalies. Its portability allows frequent patient self-monitoring outside clinical settings.

Overall, we have shown the potential of TinyMSI as an accessible, multifunctional tool for point-of-care diagnostics. It quantitatively measures blood flow, pulse rate, and oxygen levels - key physiological parameters.

Further applications of the TinyMSI system could include assessing recovery and blood flow in reconstructed tissue flaps, monitoring peripheral vascular disease in diabetes patients, and identifying vulnerable wounds in elderly populations. Its capability for frequent non-invasive monitoring of vascular health could aid early intervention and preventative therapies.

Declaration of competing interest

The authors declare the following financial interests/personal relationships which may be considered as potential competing interests: Wenyao Xu reports financial support was provided by National Institutes of Health. Wenyao Xu reports financial support was provided by National Science Foundation. Wenyao Xu is a editor for Smart Health Journal If there are other authors, they declare that they have no known competing financial interests or personal relationships that could have appeared to influence the work reported in this paper.

Data availability

The data that has been used is confidential.

Acknowledgments

This work is partly supported by the US National Institute of Health R01EB035188 and the US National Science Foundation under CNS-2050910 and OISE-2106996.

References

Armstrong, D. G., Swerdlow, M. A., Armstrong, A. A., Conte, M. S., Padula, W. V., & Bus, S. A. (2020). Five year mortality and direct costs of care for people with diabetic foot complications are comparable to cancer. *Journal of Foot and Ankle Research*, *13*, 16. http://dx.doi.org/10.1186/s13047-020-00383-2.

Bearden, J. A. (1967). X-ray wavelengths. *Reviews of Modern Physics*, *39*(78).

Delbridge, L., Perry, P., Marr, S., Arnold, N., Yue, D. K., Turtle, J. R., & Reeve, T. S. (1988). Limited joint mobility in the diabetic foot: Relationship to neuropathic ulceration. *Diabetic Medicine*, *5*, 333–337. http://dx.doi.org/10.1111/j.1464-5491.1988.tb01000.x.

Dietrich, M., Marx, S., von der Forst, M., Bruckner, Felix C. F., Fiedler, Mascha O., Nickel, F., Studier-Fischer, A., Müller-Stich, B. P., Hackert, T., Brenner, T., Weigand, Markus A., Uhle, F., & Schmidt, K. (2021). Hyperspectral imaging for perioperative monitoring of microcirculatory tissue oxygenation and tissue water content in pancreatic surgery — an observational clinical pilot study. *Perioperative Medicine*, *10*, 42. http://dx.doi.org/10.1186/s13741-021-00211-6.

Erickson, S. J., & Godavarty, A. (2009). Hand-held based near-infrared optical imaging devices: a review. *Medical Engineering & Physics*, *31*, 495–509.

Haugg, F., Elgendi, M., & Menon, C. (2022). Effectiveness of remote ppg construction methods: A preliminary analysis. *Bioengineering*, *9*(485), http://dx.doi.org/10.3390/bioengineering9100485.

Kamshilin, A. A., Miridonov, S., Teplov, V., Saarenheimo, R., & Nippolainen, E. (2011). Photoplethysmographic imaging of high spatial resolution. *Biomedical Optics Express*, *2*(996), http://dx.doi.org/10.1364/BOE.2.000996.

Kumar, M., Suliburk, J. W., Veeraraghavan, A., & Sabharwal, A. (2020). Pulsecam: a camera-based, motion-robust and highly sensitive blood perfusion imaging modality. *Scientific Reports*, *10*, 4825. http://dx.doi.org/10.1038/s41598-020-61576-0.

Li, H., Zheng, W., Pandya, A., Xu, C., Xia, J., & Xu, W. (2022). *Smartphone-based blood perfusion assessment for ulcer care* (pp. 843–844). ACM, http://dx.doi.org/10.1145/3560905.3568090.

Lind, A. R., & Williams, C. A. (1979). The control of blood flow through human forearm muscles following brief isometric contractions. *The Journal of Physiology*, *288*, 529–547.

Lowe, D. G. (2004). Distinctive image features from scale-invariant keypoints. *International Journal of Computer Vision*, *60*, 91–110. http://dx.doi.org/10.1023/B:VISI.0000029664.99615.94.

Lu, B., Dao, P. D., Liu, J., He, Y., & Shang, J. (2020). Recent advances of hyperspectral imaging technology and applications in agriculture. *Remote Sensing*, *12*, 2659.

Macwan, R., Benezeth, Y., & Mansouri, A. (2018). Remote photoplethysmography with constrained ica using periodicity and chrominance constraints. *BioMedical Engineering OnLine*, *17*, 22. http://dx.doi.org/10.1186/s12938-018-0450-3.

Moraitou, M., Pateli, A., & Fotiou, S. (2017). Smart health caring home: A systematic review of smart home care for elders and chronic disease patients. (pp. 255–264). GeNeDis 2016: Geriatrics.

Ng, L. M., & Simmons, R. (1999). Infrared spectroscopy. *Analytical Chemistry*, *71*, 343–350.

Oliver, T. I., & Mutluoglu, M. (2023). Diabetic foot ulcer. In *StatPearls*. Treasure Island (FL): StatPearls Publishing.

Pérez-Panero, A. J., Ruiz-Muñoz, M., Cuesta-Vargas, A. I., & Gónzalez-Sánchez, M. (2019). Prevention, assessment, diagnosis and management of diabetic foot based on clinical practice guidelines. *Medicine*, *98*, Article e16877. http://dx.doi.org/10.1097/MD.0000000000016877.

rim Park, Y, kyoung Shin, Y., & Eom, J. B. (2023). Non-contact oxygen saturation monitoring for wound healing process using dual-wavelength simultaneous acquisition imaging system. *Biomedical Engineering Letters*, *13*, 455–463. http://dx.doi.org/10.1007/s13534-023-00275-x.

Rublee, E., Rabaud, V., Konolige, K., & Bradski, G. (2011). Orb: An efficient alternative to sift or surf. In *2011 international conference on computer vision* (pp. 2564–2571). http://dx.doi.org/10.1109/ICCV.2011.6126544.

Ruengsakulrach, P., Buxton, B. F., Eizenberg, N., & Fahrer, M. (2001). Anatomic assessment of hand circulation in harvesting the radial artery. *Journal of Thoracic and Cardiovascular Surgery*, *122*, 178–180. http://dx.doi.org/10.1067/mtc.2001.112821, URL https://www.sciencedirect.com/science/article/pii/S002252230181196X.

Saiko, G., Lombardi, P., Au, Y., Queen, D., Armstrong, D., & Harding, K. (2020). Hyperspectral imaging in wound care: A systematic review. *International Wound Journal*, *17*, 1840–1856. http://dx.doi.org/10.1111/iwj.13474.

Sato, Y., Nakajima, S., Shiraga, N., Atsumi, H., Yoshida, S., Koller, T., Gerig, G., & Kikinis, R. (1998). Three-dimensional multi-scale line filter for segmentation and visualization of curvilinear structures in medical images. *Medical Image Analysis*, *2*, 143–168. http://dx.doi.org/10.1016/S1361-8415(98)80009-1.

Shin, B., & Lee, D. (2018). *Deep blood vessel visualization over 10-mm depth using nir light* (pp. 714–718). IEEE, http://dx.doi.org/10.1109/URAI.2018.8441817.

Tresierra-Ayala, M., & Rojas, A. G. (2017). Association between peripheral arterial disease and diabetic foot ulcers in patients with diabetes mellitus type 2. *Medicina Universitaria*, *19*, 123–126. http://dx.doi.org/10.1016/j.rmu.2017.07.002.

Zhou, R., Zhong, D., & Han, J. (2013). Fingerprint identification using sift-based minutia descriptors and improved all descriptor-pair matching. *Sensors (Basel, Switzerland*, *13*, 3142–3156. http://dx.doi.org/10.3390/s130303142.